Materials & Design 226 (2023) 111652

Contents lists available at ScienceDirect

Materials & Design

journal homepage: www.elsevier.com/locate/matdes

Exploring wettability difference-driven wetting by utilizing electrospun chimeric Janus microfiber comprising cellulose acetate and polyvinylpyrrolidone

Menglong Wang [a,c], Ruiliang Ge [b], Ping Zhao [c], Gareth R. Williams [d], Deng-Guang Yu [c,*], S.W. Annie Bligh [a,*]

[a] School of Health Sciences, Caritas Institute of Higher Education, Hong Kong, China
[b] Department of Outpatient, Third Affiliated Hospital of Navy Military Medical University, Shanghai 200438, China
[c] School of Materials and Chemistry, University of Shanghai for Science and Technology, Shanghai, China
[d] UCL School of Pharmacy, University College London, London WC1E 6BT, UK

HIGHLIGHTS

- Through a special designed spinneret, tri-fluid side-by-side electrospinning process was conducted and chimeric Janus microfiber was obtained.
- The first electrospun microfiber with wettability difference surface was used to explore the wetting process.
- The wettability difference-driven water motion provided another wetting mechanism except for water absorbance.
- By fitting four models, drug release profiles showed that they were electrospun microfiber-based sustained drug release systems.

GRAPHICAL ABSTRACT

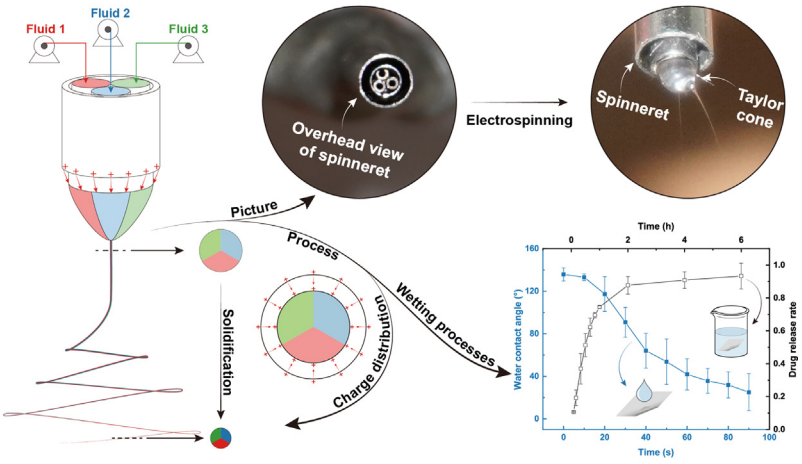

ARTICLE INFO

Article history:
Received 4 August 2022
Revised 19 January 2023
Accepted 23 January 2023
Available online 25 January 2023

Keywords:
Tri-fluid electrospinning
Chimeric Janus microfiber
Wettability
Drug release
Hydrophobic difference

ABSTRACT

In exploring the difference in the wettability of fibers with various structures, three inner constructions of fibers, namely, uniaxial, Janus and chimeric Janus, have been fabricated by electrospinning. In electrospun fibers, polyvinyl pyrrolidone and cellulose acetate were used as a polymer matrix and ketoprofen was used as a model drug. Morphologies and inner structures were respectively investigated by scanning electron microscopy (SEM) and Transmission electron microscopy (TEM). Physical states and compatibilities of materials were detected by X-ray diffraction (XRD) and Fourier transform infrared spectroscopy (FTIR). Water contact angle (WCA) tests were conducted to determine the difference between wettability and wetting time among assorted fiber membranes. Results showed that the wettability gradient could drive water movement and wetting, which resulted in the rapid decrease of the WCA, to prepare Janus and chimeric Janus fiber membranes compared with uniaxial fiber membranes. Otherwise, in vitro drug release experiments were carried out and four fitting models were applied in matching release profiles. The results showed that electrospun fiber membranes belonged to sustained-release systems and such

* Corresponding authors.
E-mail addresses: ydg017@usst.edu.cn (D.-G. Yu), abligh@cihe.edu.hk (S.W.A. Bligh).

https://doi.org/10.1016/j.matdes.2023.111652

membranes were influenced by drug diffusion and backbone corrosion effects. In this study, whether electrospun multilayer Janus fibers could affect wettability and drug release was investigated.

1. Introduction

As a fundamental property, wettability is ubiquitous in nature and our lives, where water is involved. For some plants and animals, they evolve hydrophilic or hydrophobic parts of themselves for their benefit. Some water-loving surfaces have been found from nature, such as fish scale, shark skin, spider silk and nepenthes alata. In addition, some water-repelling surfaces from animals and plants have been discovered such as duck feather, lotus, legs of water striders and butterfly wings [1]. For human interests, various artificial materials with different wettability have been designed, fabricated and applied in many fields, such as sewage treatment [2], drug delivery [3,4], sensors [5,6], lithium-ion battery [7,8], environmental remediation [9], filters [10,11] and biomedical scaffolds [12,13]. In general, with regard to drug delivery systems, a hydrophilic surface is required because water is the environment, wherein medicine can be absorbed easily.

A positive correlation between drug release rate and wettability has been proven by many reports; thus, various strategies are proposed to improve wettability of drug delivery systems [14]. When mixed into the drug carrier matrix, surfactants serve as effective small molecules in modulating the hydrophilic property [15,16]. Some active substances can also play the same role. Siranjeevi Ravichandran et al. mixed *Clerodendrum phlomidis* leaf extract into electrospun polycaprolactone (PCL) nanofibers, thereby reducing the water contact angle (WCA) from 137.4° ± 5.2° for pure PCL to 72.41° ± 2.4° for complex fiber [17]. Jaganathan et al. added Mahua oil and propolis into electrospun polyurethane scaffold and obtained a greatly improved complex wettability material and they explored its application in bone tissue engineering, which obtained good cell viability of 206.3% ± 14.36% [18]. Incorporating a hydrophilic polymer to adjust hydrophobicity/ hydrophilicity is a common and handy method [19,20]. Thus, electrospinning is usually applied because it can leave abundant and easily wetted groups on the surface of fibers. Some groups wetted with ease can vastly increase the wettability, although they were implanted on metal [21]. In some other controlled–release drug delivery systems, wettability can be changed by modulating the pH [22,23] and temperature [24,25].

Electrospinning, a simple and handy technology in preparing micro/nano fibers, has been developed for tens of years and applied to various fields [26–30] since Reneker's group carried it forward again in 1990s [31]. It has also contributed to the preparation of complex structures of micro/nano fibers [32–34]. As two fundamental structures, core–shell and Janus are basic structures in nature. Although core–shell spinneret was proposed with a traditional uniaxial spinneret by Cooley in 1902 [35], Janus spinneret and corresponding electrospinning were raised and carried out later by Gupta and Wilkes in 2003 [36]. It is separated among working solutions during electrospinning, which is difficult to be solved. Side-by-side electrospinning technology is developed slowly than coaxial electrospinning. A set of data from Web of Science indicates that the item numbers of "side-by-side electrospinning or Janus" and "coaxial electrospinning or core–shell" are 36,974 and 104,665 until July 2022. In addressing this problem, key points of this challenge should be refined. Among multilayer Janus electrospinning, more than one working solution is gathered on the tip of the structured spinneret. When solutions are not fully contacted or their contacted area is not large enough, the working fluid formed by solutions will be separated by electrostatic repulsion force. Thus, diverse strategies have been proposed. In 2017, Yu et al. designed a special structure spinneret, which has two acentric needles nested into a third metal capillary. Utilizing this spinneret, Janus nanofiber has been prepared with a smooth surface. In another experiment, an extra solvent used as a sheath to protect solutions from separation [37]. Therefore, increasing the contact area between working solutions or separating charge from working solutions can enhance the stability of side-by-side electrospinning. Otherwise, in 2019, Cai et al. proposed a dual spinneret penetrating through the center of a small round metal sheet, which can bind working solutions [38]. An additional electric field is used to allow working solutions to contact sufficiently. Therefore, sufficient contact among working solutions is the key point to conduct side-by-side electrospinning.

Polyvinyl pyrrolidone (PVP), a non-toxic, biocompatible, chemically inert and non-ionic polymer, is widely used in drug delivery systems [39,40], cosmetics [41] and nanoparticle carriers [42]. Cellulose acetate (CA), the acetate ester of cellulose, has various advantages such as biocompatibility, biodegradability, regenerative property and high affinity. It has been broadly applied in many fields [43–45]. PVP and CA are frequently used hydrophilic materials. In addition, they are both electrospinnable with appropriate molecular weight and concentration. The combination of PVP and CA applied to the drug delivery system through electrospinning has been explored for many times. Edikresnha et al. electrospun PVP/CA composite nanofiber without loading glycerin and reported that garlic extract performed good wettability [46]. Tsekova et al. prepared a curcumin-loaded CA/PVP fibrous membrane to promote drug release. The WCA for different prepared fibers was recorded simultaneously with water droplet deposition, 129.4° ± 3.8° for pure curcumin CA and 14.8° ± 1.7° for curcumin-loaded CA/PVP fibrous mat [47]. Castillo-Ortega et al. fabricated an amoxicillin/CA@CA/PVP core–shell fiber utilizing coaxial electrospinning. This membrane performed a fast release in tens of minutes indicating its good wettability [48]. As pure CA fiber mats usually possess lower hydrophilic property and need longer wetting time than PVP, they can easily dissolve into most inorganic and organic solvents. PVP is a user-friendly material that can be mixed with CA to improve its wettability. However, there are few works on building a wettability difference fiber surface. As uniaxial electrospinning technology was not easy to realize this special structure. Thus, Janus structure, especially multilayer Janus structure, should be applied for this design. Otherwise, the combination of mixing easy hydrophilic materials and constructing wettability gradient surface will further improve wettability of fibrous membrane.

In this work, for addressing the separation among working solutions, a specially designed complex structured spinneret was used. In this spinneret, a metal tube netted with a side-by-side structure protrudes a certain length to ensure that working solutions can be contacted adequately. In addition, the out-most metal tube can serve as an additional electro field [38]. KET, a commonly used nonsteroidal anti-inflammatory drug [49], was applied as a model drug in exploring release behavior of different kinds of fiber membranes. PVP and CA were used as a polymer matrix. By dissolving the different concentrations of these two polymers, different working solutions can be prepared and utilized for fabricating uniaxial, Janus and chimeric Janus microfibers through the special designed spinneret. Thus, wettability difference can be constructed on the

fiber surface, particularly for chimeric Janus fiber comprising three sections with various wettability. This wettability difference will play a similar role as the wettability gradient on the cactus spines, which can promote the self-motion of water and decrease the WCA [50]. Wetting processes were recorded with the results showing that Janus and chimeric Janus fiber membranes performed better wettability than the PVP-CA uniaxial fiber. Driven by wettability gradient, Janus and chimeric Janus fibers showed improved wetting performance. As electrospun nanofibers have been widely explored in drug delivery systems [51–54], in vitro drug release experiments were further conducted to explore the effect of wetting speed on drug release profiles.

2. Materials and methods

2.1. Materials

Cellulose acetate (CA, Mn ~ 30,000) and polyvinylpyrrolidone (PVP K60, average mol wt ~ 360,000) were purchased from Sigma Aldrich (Shanghai) Trading Co., Ltd., China. Ketoprofen, which is the model drug (purity > 98%, GC grade), was provided by Shanghai Macklin Biochemical Technology Co., Ltd., China. Acetone, ethyl alcohol, dimethylacetamide and phosphate-buffered saline (PBS) were obtained from Sinopharm Chemical Reagent Co., Ltd., China. All solvents were analytically pure (purity > 99.8%). Water utilized was double distilled.

2.2. Fiber preparation

The whole process of this research is shown in Fig. 1. Working solutions were prepared on the basis of a diluted drug solution, dissolving 1%(w/v) KET into a mixed solvent: acetone/alcohol/DMAc = 4:1:1(v/v/v). Fluid 3 was obtained by adding 10% (w/v) CA into the diluted drug solution. If 8% (w/v) CA and 4% (w/v) PVP K60 or 8% (w/v) CA and 2% (w/v) PVP K60 were added into the prior diluted solution, then Fluid 1 or Fluid 2 would be prepared. Their flow rate in each process, average diameters, structures and theoretical contents of different components of fiber products are listed in Table 1.

The spinneret used in this research is shown in Fig. 2(a–c). Three tiny metallic capillaries were embedded into a 14G metallic needle. A 3 * 0.15 mm (external diameter * wall thickness) metallic tube was set at the outer most to provide an appropriate electrostatic repulsion to constrain working solutions from separation and stretch working fluid. When three appropriate solutions flow past suitable channels, core–shell fibers with a chimeric Janus core were obtained under electrospinning. In this research, the connection modes in which different solutions flow through corresponding channels for various electrospinning processes are shown in Fig. 2(d–f).

In every electrospinning, four equipment were used. Pumps (KDS100, KDS200, Cole Parmer, USA) drive working solutions to gather on the tip of the specially designed spinneret. Under electric field force, which is generated by a high-voltage electrostatic generator (ZGF-60 kV/2 mA, Electric Power Automation Co. Let., China), the working fluid was ejected from the Taylor cone formed at the tip of the spinneret when electrostatic repulsion had exceeded the interaction among working solutions (Fig. 2g). Afterward, a straight jet was followed by. Then, working fluid would experience bending and swing stage to stretch working fluid into nano/micro scale (Fig. 2h). Finally, the working fluid was solidified into fiber and collected by a collector. For all electrospinning processes, collected distance and high voltage were kept at 20 cm and 8.5 kV, respectively.

2.3. Characteristics

Among electrospinning processes, a digital camera (Sony Alpha 6400) was used to picture different processes. The morphology and inner structure of microfibers were observed by using a field-emission scanning electron microscope (FESEM; Quanta FEG450, FEI Corporation, USA) and transmission electron microscope (TEM; JEM 2200F, JEOL, Japan). The diameter of microfibers was measured by using ImageJ (National Institutes of Health, USA). In obtaining the average diameter of fibers, 100 places were ran-

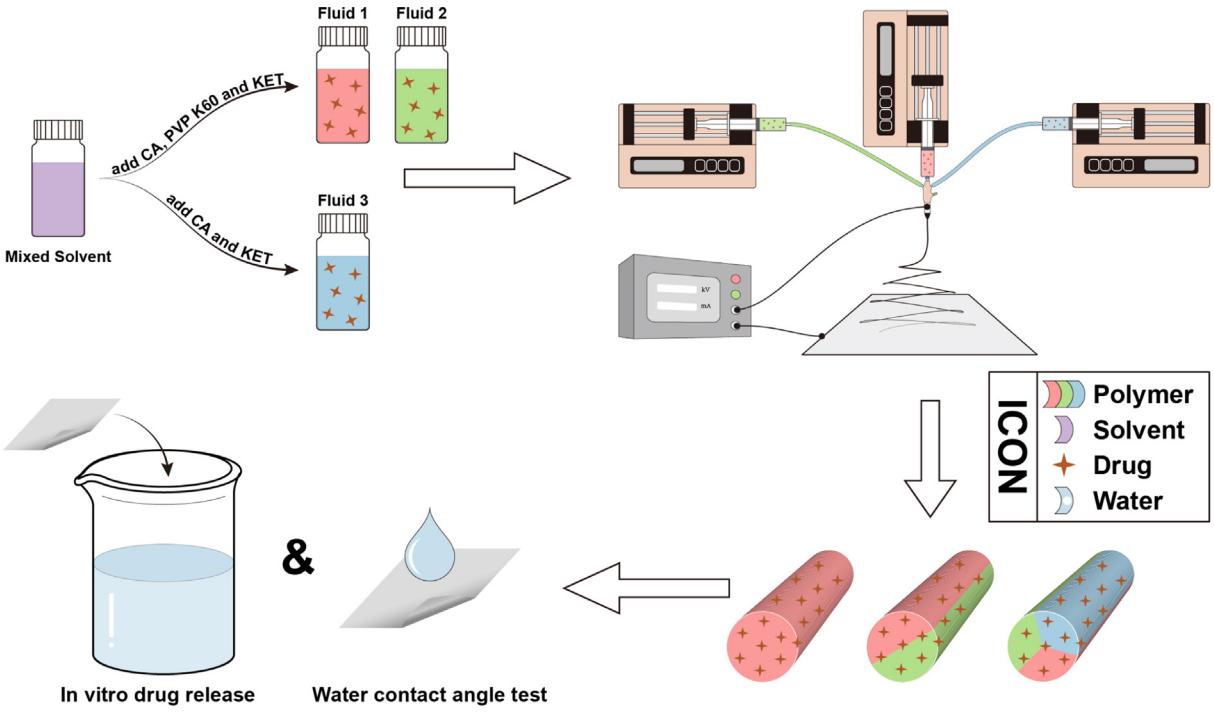

Fig. 1. Solution preparation and electrospinning for different structural microfibers and characterizations.

Table 1
Experimental scheme and corresponding parameters.

No.	Electrospinning	Flow rates (mL/h)			Average diameter (mean ± S.D. μm)	Structure	Fiber contents (%, w/w)		
		Fluid 1	Fluid 2	Fluid 3			KET	PVP	CA
F1	Uniaxial	1.2	–	–	1.210 ± 0.412	Monolithic	7.692	30.769	61.539
F2	Side-by-side	0.6	–	0.6	1.225 ± 0.215	Janus	8.333	16.667	75.000
F3	Tri-fluid side-by-side	0.4	0.4	0.4	1.370 ± 0.280	Chimeric Janus	8.571	17.143	74.286

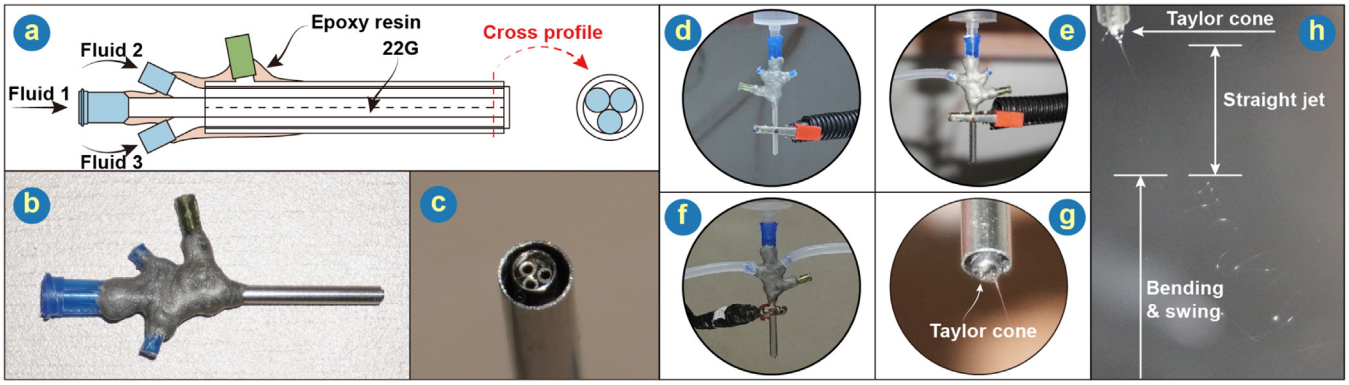

Fig. 2. (a) Graphic and (b) picture of a specially designed complex spinneret; (c) an enlarge picture of the tip of the special designed spinneret; three connection modes of electrospinning: (d) uniaxial (F1), (e) side-by-side (F2) and (f) tri-fluid side-by-side (F3); (g) a picture of a tri-fluid Taylor cone; (h) three stages of electrospinning from tri-fluid side-by-side electrospinning.

domly selected in each SEM image. The results were recorded as mean ± S.D.

Surface tension and viscosity of three working solutions were tested by surface tension meter (Kruss K100C-MK2, Germany) and rotary viscosity instrument (SNB-2, China), respectively. The surface tension tests were referred to GB/T 22237-2008 and viscosity tests were referred to GB/T 2794-2013. Otherwise, the viscosity tests were conducted under room temperature and 3# rotor with 6 rpm speed.

The physical states and interactions among molecules of raw materials and products were discovered using an X-ray powder diffractometer (XRD; AXS, Bruker, Germany) and reflectance-Fourier transform infrared (ATR-FTIR; Spectrum 100, Perkin-Elmer, USA), respectively. In XRD tests, data were collected among 10°–60° and 5° per minute. As for ATR-FTIR tests, data were gathered from 400 cm^{-1} to 4000 cm^{-1} in a step of 4 cm^{-1}. Differential scanning calorimetry (DSC, MDSC 2910, TA Instruments Co., DE, USA) was used to detect the thermodynamic property of raw materials and F3 microfiber. DSC data was collected from 70 ℃ to 220 ℃, 10 ℃ per minute.

In wettability tests of fiber membranes, an interfacial tension measuring apparatus (JC2000C1, Shanghai Zhongchen Digital Technology Apparatus Co., Ltd., China) was applied. For each sample, five different positions were tested and the results were recorded as mean ± S.D. (n = 5). For every test, approximately 5 μL of deionized water was dropped on the fiber membrane at room temperature. The reaction was observed for 3 min and recorded by using a built-in camera.

Studies on in vitro drug release were carried out in a constant-temperature water bath shaker. Based on Chinese pharmacopoeia (2015th), 0.1 g of membrane was added to 450 mL of PBS (pH 7.4). After drawing 4 mL of solution at a series of predetermined time, blank PBS with the same volume was injected into the solution. The percentage (P) of drug released from fibers can be calculated using Eq. (1).

$$P = \frac{V_0 c_n + \sum_{i=1}^{n-1} c_i V}{Q} \quad (1)$$

where V_0 is the volume of the solution equals to 450 mL; V is the volume collected at each time, which is equal to 4 mL. Q is the theoretical amount of drug in 0.1 g of fiber membrane. In addition, c_n is the drug concentration at predetermined time, which can be calculated using Beer's law as shown in Eq. (2).

$$A = \varepsilon c l \quad (2)$$

where A is the absorbance that can be detected using an ultraviolet–visible spectrophotometer (UV–Vis; Unico Instrument Co., Ltd., China) and c is the concentration. ε and l are the absorption coefficient and optical length, respectively. In this research, they are both constants.

3. Results and discussions

3.1. Morphology and inner structure of microfibers

In traditional Janus electrospinning, caused by electrostatic repulsion, working fluid integrated by different working solutions is easily bifurcated. Given the special design of the spinneret, Janus and chimeric Janus fibers were fabricated. On the one hand, the middle tube of the spinneret protrudes approximately 0.2 mm than the inner capillary; this design can facilitate contact among working solutions. On the other hand, an outer-most metallic tube was set to constrain working solutions from separating. By using this specially designed spinneret, working solutions can contact one another more adequately than those in traditional tri-fluid side-by-side electrospinning.

Thus, microfibers prepared by various electrospinning processes show a smooth surface morphology and relative uniform diameter size distribution (Fig. 3). Microfibers obtained from side-by-side and tri-fluid side-by-side electrospinning performed good size distribution with 1.225 ± 0.215 μm (R^2 = 0.99433) and 1.370 ± 0.280 μm (R^2 = 0.98231), respectively.

The inner structures of Janus fiber can be observed from TEM images. As shown in Fig. 4a, the two sides of a Janus fiber measured 418.137 and 246.480 nm. The boundary line formed by different gray levels of two sides is easy to distinguish. As the flow rates

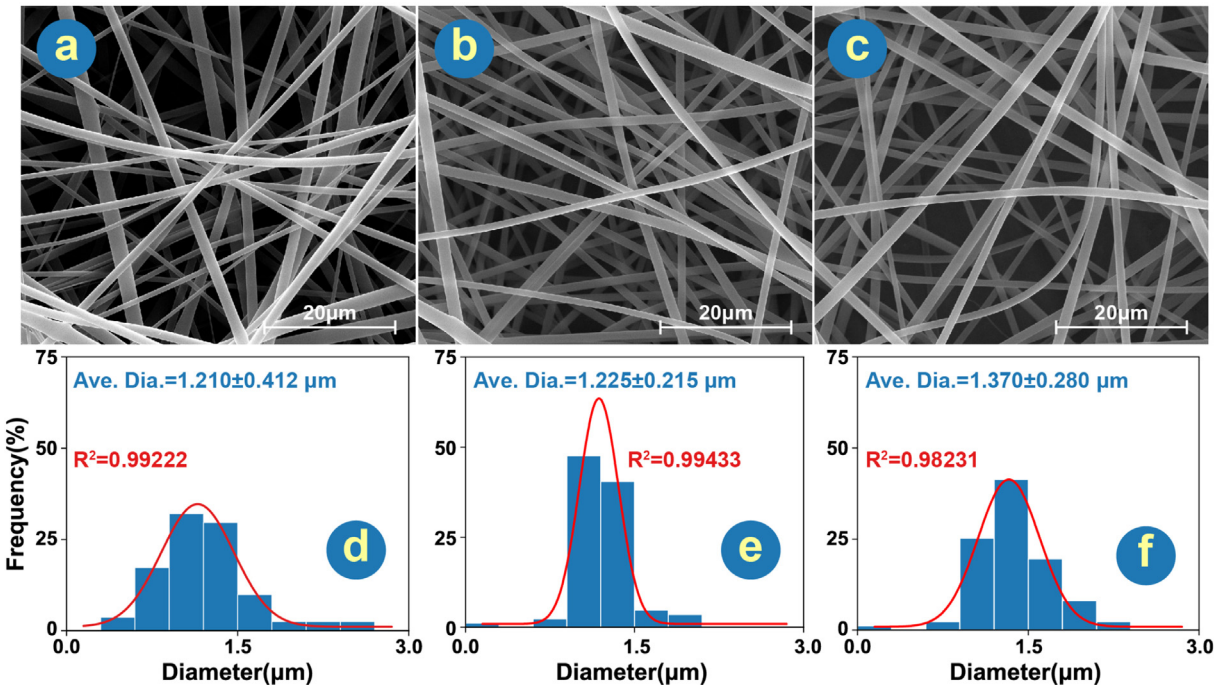

Fig. 3. SEM images and diameter distribution of different microfibers: (a) and (d) for uniaxial fiber; (b) and (e) for Janus fiber; (c) and (f) for chimeric Janus fiber.

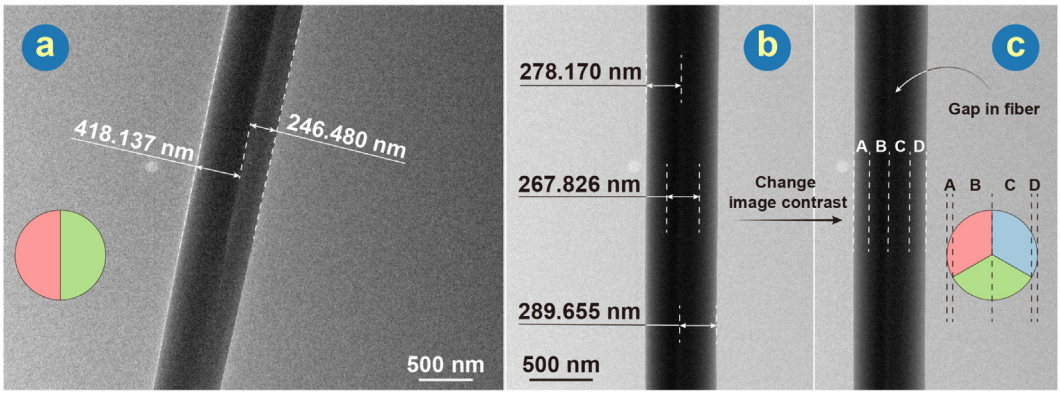

Fig. 4. TEM images of different Janus microfibers. (a) Janus microfiber; (b) and (c) chimeric Janus microfiber.

are equal, their size difference may be due to different concentrations. The chimeric Janus fiber can be observed in Fig. 4b with sides measuring approximately 278.170, 267.826 and 289.655 nm. As the chimeric Janus structure is not easily identified in Fig. 4b, a contrast-changed image (Fig. 4c) was provided for better observation. A gray gap closed to the center is displayed in the dark fiber. This structure might have three sides, two at the front and one at the back.

In tri-fluid side-by-side electrospinning, three sections with different ratios of polymers were integrated into one microfiber. Thus, forming a clear boundary from an overhead view is difficult, as different sections are overlapped. Different sections (A, B, C and D) marked on a chimeric Janus microfiber (Fig. 4c) are highlighted in the inset. As for the gap between B and C sections, the combination among them can be weak, thereby forming an area through which electron beam can pass. The weak combination is due to fast solidification, which limited working solutions flowing into one another. Thus, by utilizing the specially designed spinneret and under appropriate parameters, electrospinning was successfully carried out, then a series of uniform microfibers was obtained.

3.2. Details on chimeric tri-layer side-by-side electrospinning

By combining a traditional tri-layer side-by-side electrospinning and strategies on avoiding fluid splitting, chimeric tri-layer side-by-side electrospinning was carried out in preparing chimeric Janus microfibers composed of three different parts. Given the middle metallic capillary, which packs three 22G needles flowing through working solutions and protrudes a short length, after working solutions flow out from inner-most needles, they will effectively contact before forming a Taylor cone. As the protrude length is short, working solutions cannot be mixed. Along with the three stages of electrospinning, namely, Taylor cone, straight jet and bending and swing, solvent was gradually removed from the working fluid, which finally transformed into a microfiber (Fig. 5a). In the Taylor cone stage, charges distributed on the edge of the out-most metallic tube are similar to those distributed on the surface of the working fluid. The electrostatic repulsion generated has two effects (Fig. 5b): constraining working solutions from splitting and stretching working fluid to promote Taylor cone to straight jet. As electrospinning develops, the working fluid moves

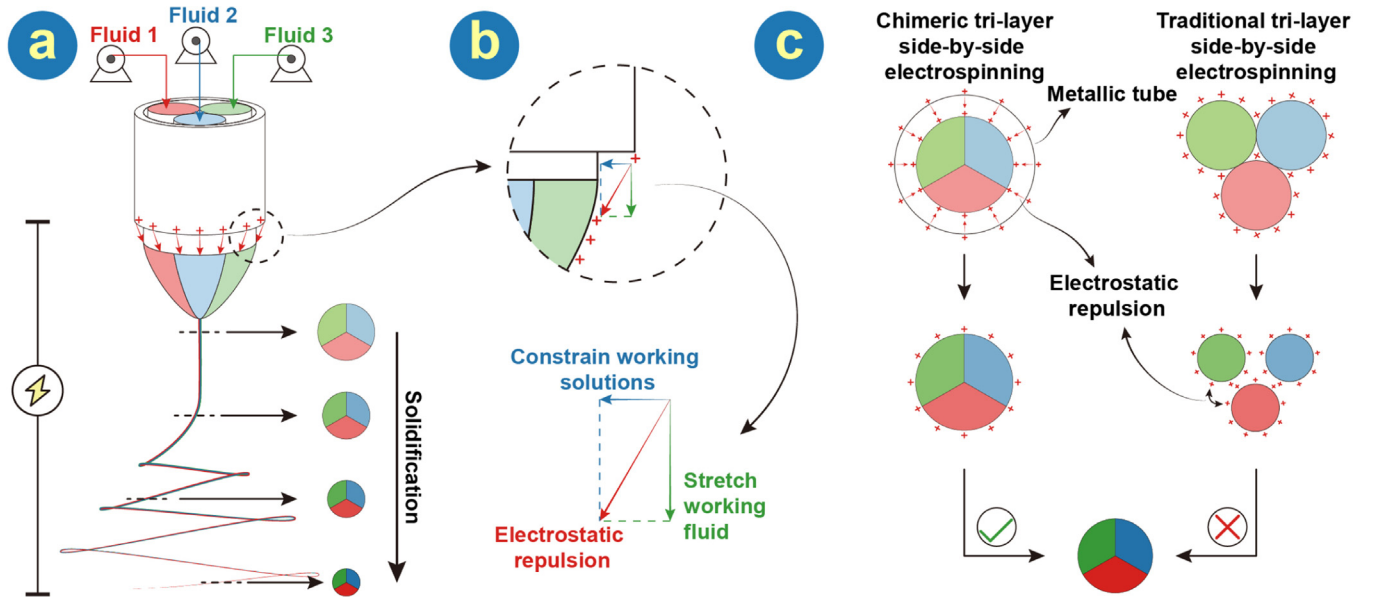

Fig. 5. (a) Illustration on chimeric tri-layer side-by-side electrospinning; (b) the form that electrostatic repulsion acted on the Taylor cone; (c) a comparison of charge distribution between chimeric tri-layer side-by-side electrospinning and traditional tri-layer side-by-side electrospinning.

farther from the spinneret. Influences, which acted on the working fluid, from electrostatic repulsion are decaying. Consequently, working fluid composed of working solutions integrated by condensed solutions will be partly removed from the preceding course. Therefore, condensed working fluid with a robust connection among working solutions cannot be departed by electrostatic repulsion before the formation of chimeric Janus fibers. Surface tension and viscosity of three working solutions were listed in Table S1.

By comparing traditional side-by-side electrospinning with tri-fluid electrospinning, the traditional one is often severely affected by electrostatic repulsion, which will split working fluid up before it solidifies (Fig. 5c). Thus, a traditional process cannot effectively form tri-layer Janus fibers. However, in this work, a St20;"pecially designed spinneret was used to carried out chimeric tri-layer side-by-side electrospinning, thereby preventing the splitting of the working fluid. Along with solidification, working fluid removes solvent gradually and finally forms fibers with a chimeric Janus structure.

3.3. Chemical and physical states of microfibers

As a classic crystal medicine, KET has various sharp peaks that can be observed from its XRD pattern (Fig. 6a). On the contrary, polymers, such as CA and PVP, who do not have a long-range order structure, serve as humps on their patterns. Electrospinning can transfer matter from crystal into amorphous state; thus, the XRD pattern of microfiber membranes shows an amorphous form.

FTIR curves indicate compatibility among materials. As shown in Fig. 6b, the PVP spectra that peaks at 1651 and 1423 cm^{-1} correspond to the stretching vibration of the carbonyl group in amide and C–H bending vibration of CH_2. In addition, C-N stretching peaks at 1284 cm^{-1}. A broad band at approximately 3427 cm^{-1} represents the O–H bond [55]. In the CA spectrum, several peaks related to the acetyl group emerge, such as C=O stretching (1727 cm^{-1}), C–H bending of $-CH_3$ (1365 cm^{-1}) and C-O stretching (1219 cm^{-1}). Otherwise, as the backbone bond, the absorbance peak of C-O-C arises at 1035 cm^{-1} [56,57].

Based on the FTIR spectrum of KET, two absorbance peaks of stretching vibrations, 1694 and 1654 cm^{-1}, from C=O can be easily observed: one from the carboxyl group and the other from the ketonic group [58,59]. However, in membranes' spectra, index peaks cannot be well distinguished because the model drug was dispersed uniformly in fiber after having been electrospun. Some red shifts are also observed compared with raw materials, for example, 1651 cm^{-1} in PVP transfers to 1658 cm^{-1}; 1727, 1365 and 1219 cm^{-1} in CA transfers to 1743, 1370 and 1227 cm^{-1}, respectively. The findings revealed that some proton acceptors as C=O, C-O can interact with proton donors such as O–H [60]. DSC data also supports the results form XRD and FTIR (Fig. S1).

3.4. Wetting ability of different microfibers

Wettability is an important performance for medicated fibers. When medicine-loading fiber membranes were soaked in water, this property will affect drug release profiles. Therefore, before conducting in vitro experiments, wetting tests had been carried out to investigate wetting time for F1 to F3 microfibers. The results are shown in Fig. 7a. Compared with F1, F2 and F3 exhibit higher WCA at 135.6728° ± 3.3694° and 135.7270° ± 6.2137° and quickly decrease to 8.1438° ± 14.5002° and 19.5269° ± 18.3367°, respectively, in 90 s. Uniaxial microfiber, F1, had the lowest WCA (120.7271° ± 3.2825°) at the beginning. Its hydrophobic performance can last 70 s, which is two times longer than that of F2 and F3. After 3 min, it will decrease to 22.9380° ± 4.4291°.

After the first model proposed by Young in 1805, the second model, which considered solid surface roughness, was raised by Wenzel in 1936. Cassie proposed the third wetting model, Cassie's model, which introduce air into the gap between liquid and solid [61]. Apart from the two previous models, Cassie's model is static (Fig. 7b). In this work, the WCAs are not the same all the time. In the first tens of seconds, Cassie's model works well because electrospun microfiber membranes have many pores. Considerable air is found between liquid and solid. The WCA of F2 and F3 was slightly higher than that of F1 probably because of the high CA content on the fiber surface. The reason of low WCA should be slightly different from that in the F1 membrane. In the presence of a wettability gradient, F2 and F3 have two and three sections with different wettability, respectively. On the surface of the Janus fiber, the effective gradient from hydrophobic to hydrophilic is the same in

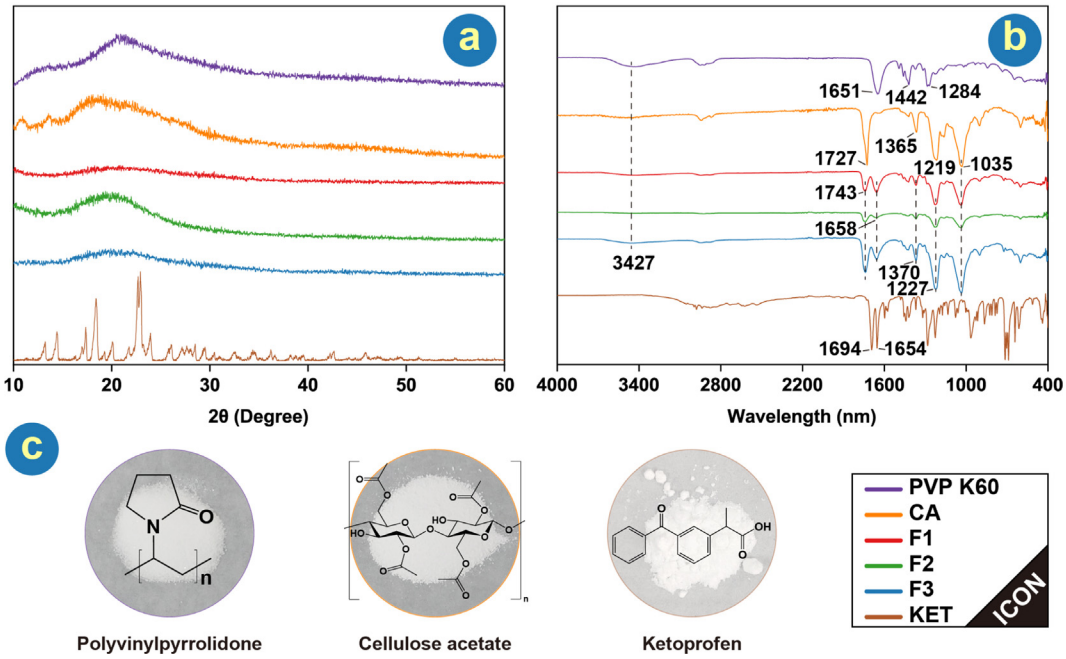

Fig. 6. (a) XRD patterns and (b) FTIR curves of raw materials and microfiber membranes; (c) structural formulas and digital pictures of untreated materials.

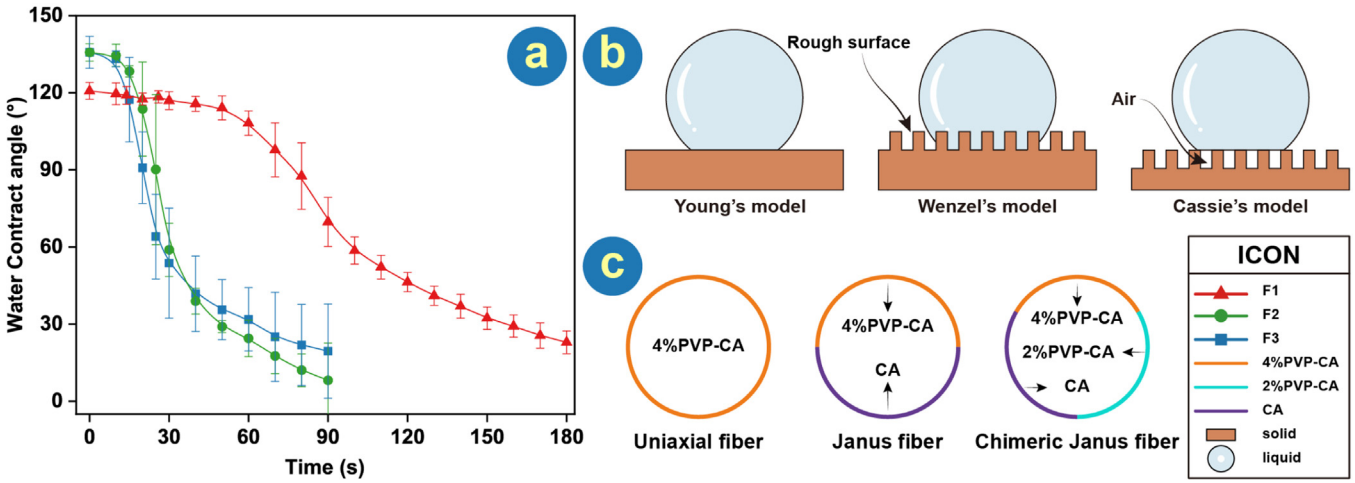

Fig. 7. (a) Wetting for three microfiber membranes; (b) different wetting models; (c) different components occupied the surface area for three kinds of fibers.

different directions. However, it is various in different directions on the surface of the chimeric Janus fiber (Fig. 7c). Based on published reports, the wettability difference could promote wetting [62]. Furthermore, some published articles demonstrated that water movement can be driven by wettability gradient [63]. Thus, for Janus and chimeric Janus fibers, wetting rather than water absorption should be considered. The wettability gradient-driven wetting will spread water, thereby covering the surface of the microfiber. A considerable amount of water is needed to wet fibrous membranes because of the huge specific surface area granted by electrospinning, thereby causing a quick reduction in WCA.

The other reason is water absorption based on the surface energy theory. With a high binding energy, the carbonylic group originated from pyrrolidone in PVP is an excellent hydrophilic group. Although the carbonylic group originated from ester, CA has a low binding energy group, methyl, as its end group. As electrospinning can keep various groups on the surface of fibers. In this work, for uniaxial microfiber, abundant methyl groups will decrease its surface energy, thereby lowering the speed of wetting [21]. However, for F2 and F3, they will take more time to absorb water because their surfaces have a larger percentage of CA than F1. Therefore, for uniaxial fiber membrane, wetting and water absorption could decrease the WCA. However, for Janus and chimeric Janus fiber membranes, wetting dominates the quick reduction of WCA, after that water absorption decreases.

3.5. In vitro drug release profiles

In vitro drug release experiments were carried out by utilizing the standard curve shown in Fig. 8a, which is fitted by a series of data gathered by using an UV–vis spectrophotometer at approximately 260 nm with a set of determined KET concentrations. Drug release profiles in 6 h and 60 min have been shown in Fig. 8b and 8c, respectively. Drug release rates for all three microfiber membranes can nearly complete release. It only takes 60 min to release

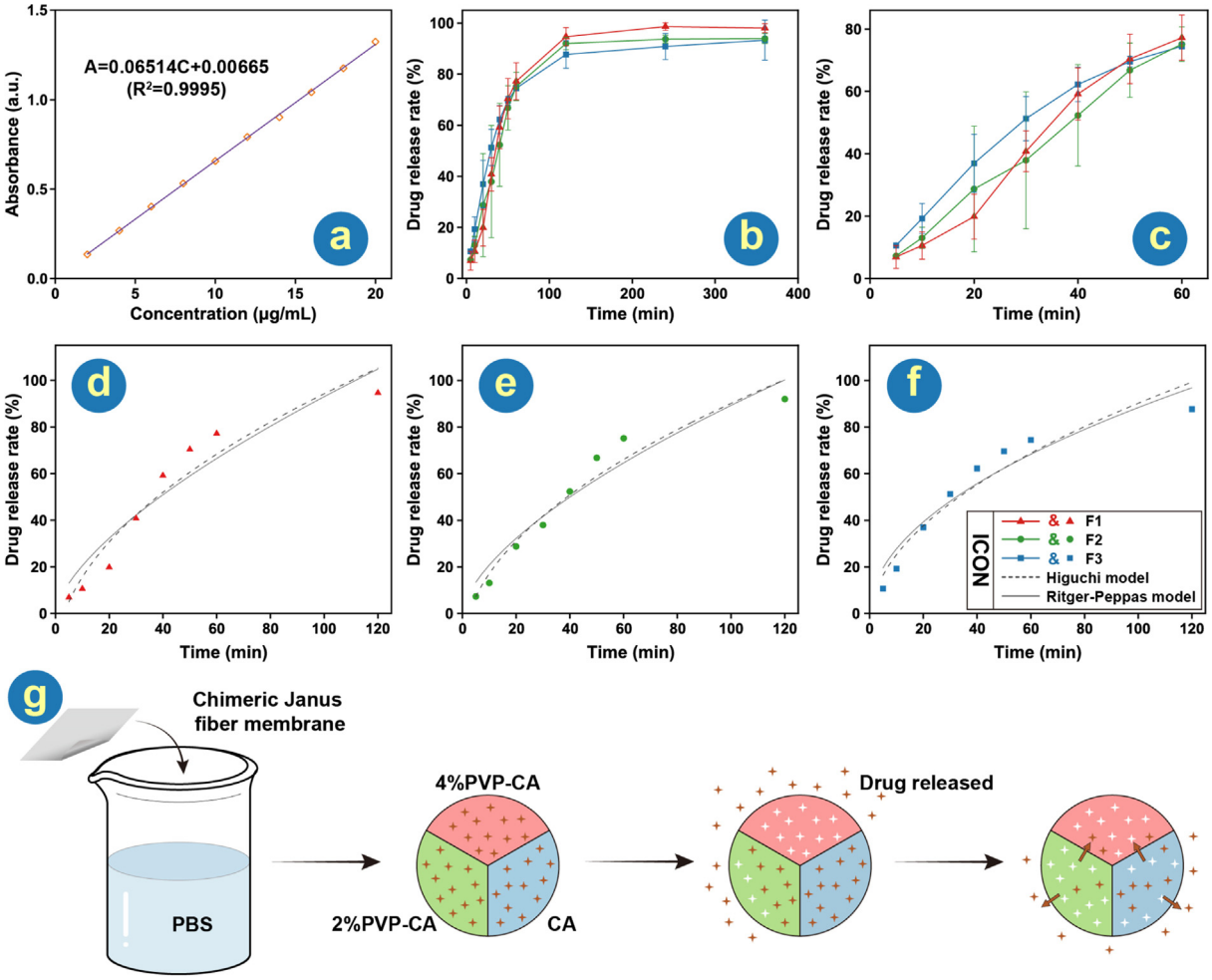

Fig. 8. (a) Standard curve of KET at 260 nm; (b) drug release profiles of three microfiber membranes in 6 h and (c) the first 60 min drug release; based on drug release profiles, two fitting models (Higuchi model and Ritger–Peppas model) were used to match data of (d) uniaxial, (e) Janus and (f) chimeric Janus microfibers; (g) an illustration on the drug release of the chimeric Janus fibrous membrane.

about 80% of the three kinds of membranes. Furthermore, 5 h was needed to release the rest of the membranes.

As shown in Fig. 8c, during the first 20 min, F2 and F3 performed faster release than F1 because of the different wetting time of microfiber membranes. F2 and F3 were wetted faster than F1; thus, drug is released quicker. In addition, the release rate of F1 surpassed F2 and F3 at around 60 min and sustained to the end. When three kinds of fibers are all immersed in water, F2 and F3 fibers performed slower release than F1 because they possess a lower content of PVP compared with F1, which is a classic fast-release excipient.

Four drug release models, including Zero-order, First-order, Higuchi and Ritger–Peppas models, were used to match the data from drug release profiles of three kinds of fiber membranes and further explore the drug release. Their equations are described as follows.

Zero-order model:

$$Z(t) = M_t/M_\infty = k_0 t + Z_0 \tag{3}$$

First-order model:

$$\ln(1 - M_t/M_\infty) = -k_1 t \tag{4}$$

This model can transform into another format that is uniformed with others.

$$F(t) = M_t/M_\infty = F_0(1 - e^{-k_1 t}) \tag{5}$$

Higuchi model:

$$H(t) = M_t/M_\infty = k_2 t^{1/2} + H_0 \tag{6}$$

Ritger–Peppas model:

$$RP(t) = M_t/M_\infty = k_3 t^n \tag{7}$$

where M_t and M_∞ are the cumulative release amount at t and ∞ time, respectively; $Z(t)$, $F(t)$, $H(t)$ and $RP(t)$ are the functions of t, representing the cumulative release rate; k_0, k_1, k_2, k_3, Z_0, F_0, H_0 and n are all constants.

The obtained fitting functions and their standard deviations are listed in Table 2. In the data used, the first 2 h was cut out from release profiles, whereas the release rates at 2 h nearly reached the maximum. As the three kinds of microfiber membranes are not drug controlled–release systems, the zero-order model did not perform well. First-order and Higuchi models were designed for the sustained-release system; thus, they had two highest standard deviations. This result indicates that the three fiber membranes belong to sustained-release systems. Furthermore, based on Ritger–Peppas functions, n value revealed the drug release method. For all three release profiles, n values, F1 with 0.6573, F2 with 0.6337 and F3 with 0.5038, are all between 0.45 and 0.89, indicating that drug diffusion and corrosion backbone effects are involved in drug release. It can be easily understood that PVP is

Table 2
Fitting functions and standard deviations from four models.

Models	Zero-order	First-order	Higuchi	Ritger–Peppas
F1	$Z(t) = 13.3230 + 0.8152*t$ ($R^2 = 0.8324$)	$F(t) = 115.9678*(1-\exp(-0.0160*t))$ ($R^2 = 0.9588$)	$H(t) = 11.5009*t^{1/2} - 20.7454$ ($R^2 = 0.9357$)	$RP(t) = 4.5080*t^{0.6573}$ ($R^2 = 0.8324$)
F2	$Z(t) = 14.7790 + 0.7613*t$ ($R^2 = 0.86.23$)	$F(t) = 109.9785*(1-\exp(-0.0166*t))$ ($R^2 = 0.9819$)	$H(t) = 10.6890*t^{1/2} - 16.7322$ ($R^2 = 0.9600$)	$RP(t) = 4.8233*t^{0.6337}$ ($R^2 = 0.9384$)
F3	$Z(t) = 24.0695 + 0.6556*t$ ($R^2 = 0.7849$)	$F(t) = 92.5274*(1-\exp(-0.0268*t))$ ($R^2 = 0.9973$)	$H(t) = 9.5072*t^{1/2} - 4.8594$ ($R^2 = 0.9322$)	$RP(t) = 8.6840*t^{0.5038}$ ($R^2 = 0.9264$)

a frequently used water-soluble material and CA is a well-known hydrophilic swelling polymer.

Based on the wetting data, drug release profiles can be clarified. Different from Janus and chimeric Janus fibers, as a homogeneous fiber, F1 fabricated by uniaxial electrospinning was wetted gradually. Water was absorbed by a fibrous membrane slowly in the first several minutes. Meanwhile, drug was released through a diffusion and backbone corrosion mechanism. By contrast, F2 and F3 membranes preferred to be wetted initially by a wettability gradient among different sections, accompanied with drug release. Similar to the Janus microfiber, in chimeric Janus microfibers, drug was gradually released into PBS from 4%PVP-CA, 2%PVP-CA and CA sections in sequence (Fig. 8g).

4. Conclusions

In this research, by using a specially designed complex spinneret, three electrospinning processes have been carried out and uniaxial, Janus and chimeric Janus microfibers were obtained. Under the same high voltage, collected distance and total flow rate, microfibers with different structures have similar average diameter. XRD and FTIR spectra show fibers made from raw materials with good compatibility and hydrogen bond formed among them. As the newly prepared microfiber, chimeric Janus fiber has three sections from three different working solutions. With different ratios between PVP and CA, the wettability gradient is formed within a microfiber. Wettability gradient-driven wetting and water movement theories were used to explain the difference on decreasing the WCA of various fiber membranes. Given this wettability gradient, the chimeric Janus fiber performed quick decrease on WCA and fast drug release at the earlier stage. Four fitting models were used to match drug release profiles, finding that all of the three membranes belonged to sustained-release systems. Furthermore, the Ritger–Peppas model revealed that they were in accordance with the release, which is affected by backbone corrosion and drug diffusion effects.

For a long-term perspective, two strategies for wettability improvement including constructing wettability-difference surface and easy hydrophilic material addition can be incorporated into chimeric Janus fibers. Thus, this tri-fluid electrospinning technology should be a robust platform for other applications, such as fog harvesting membranes and humidity sensors.

Data availability

Data will be made available on request.

Declaration of Competing Interest

The authors declare that they have no known competing financial interests or personal relationships that could have appeared to influence the work reported in this paper.

Acknowledgements

This work was supported by the Hong Kong Research Grant Council (No. UGC/FDS11/P01/21) and the Natural Science Foundation of Shanghai (No.20ZR1439000). SWAB thanks the support of Institutional Strategic Grant of the Caritas Institute of Higher Education (ISG190101).

Appendix A. Supplementary material

Supplementary data to this article can be found online at https://doi.org/10.1016/j.matdes.2023.111652.

References

[1] Y. Si, Z. Dong, L. Jiang, Bioinspired designs of superhydrophobic and superhydrophilic materials, ACS Cent. Sci. 4 (9) (2018) 1102–1112, https://doi.org/10.1021/acscentsci.8b00504.
[2] R. Zhu, M. Liu, Y. Hou, D. Wang, L. Zhang, D. Wang, S. Fu, Mussel-inspired photothermal synergetic system for clean water production using full-spectrum solar energy, Chem. Eng. J. 423 (2021), https://doi.org/10.1016/j.cej.2021.129099 129099.
[3] G. Liu, S. Xu, Y. Liu, Y. Gao, T. Tong, Y. Qi, C. Zhang, Flexible drug release device powered by triboelectric nanogenerator, Adv. Funct. Mater. 30 (12) (2020) 1909886, https://doi.org/10.1002/adfm.201909886.
[4] H.V. Ngo, P.H.L. Tran, B.-J. Lee, T.T.D. Tran, The roles of a surfactant in zein-HPMC blend solid dispersions for improving drug delivery, Int. J. Pharm. 563 (2019) 169–173, https://doi.org/10.1016/j.ijpharm.2019.04.009.
[5] C. Song, Z. Zhao, Y. Lin, Y. Zhao, X.-Y. Liu, C. Lin, C. Wu, A nanoneedle-based reactional wettability variation sensor array for on-site detection of metal ions with a smartphone, J. Colloid Interface Sci. 547 (2019) 330–338, https://doi.org/10.1016/j.jcis.2019.04.015.
[6] C. Lu, H. Li, S. Yu, Z. Jiao, L. Li, Ridged Zn/PDMS smart surface with wide-range reversible wettability and high sensitivity responsive to mechanical strain, Mater. Des. 193 (2020), https://doi.org/10.1016/j.matdes.2020.108857 108857.
[7] A. Davoodabadi, C. Jin, D.L. Wood Iii, T.J. Singler, J. Li, On electrolyte wetting through lithium-ion battery separators, Extreme Mech. Lett. 40 (2020), https://doi.org/10.1016/j.eml.2020.100960 100960.
[8] T. Dong, Z. Yu, J. Choi, K. Yoo, J. Shim, T.J. Ko, Lithium-ion battery separator prepared by double-matrix encapsulation and penetration, ACS Appl. Energ. Mater. 4 (6) (2021) 6062–6073, https://doi.org/10.1021/acsaem.1c00908.
[9] A. Shome, J.C. Moses, A.M. Rather, B.B. Mandal, U. Manna, Unconventional and facile fabrication of chemically reactive silk fibroin sponges for environmental remediation, ACS Appl. Mater. Interfaces 13 (20) (2021) 24258–24271, https://doi.org/10.1021/acsami.1c03150.
[10] N. Bakhtiari, S. Azizian, B.F. Mohazzab, B. Jaleh, One-step fabrication of brass filter with reversible wettability by nanosecond fiber laser ablation for highly efficient oil/water separation, Sep. Purif. Technol. 259 (2021), https://doi.org/10.1016/j.seppur.2020.118139 118139.
[11] F. Zhang, X. Pei, K. Zhai, C. Wang, Y. Bai, B. Zhang, Y. Wang, Y. Tan, K. Xu, P. Wang, Starch-based nanospheres modified filter paper for O/W emulsions separation and contaminants removal, Int. J. Biol. Macromol. 162 (2020) 1118–1126, https://doi.org/10.1016/j.ijbiomac.2020.06.233.
[12] Y. Mao, R. Guidoin, Y. Li, G. Brochu, Z. Zhang, L. Wang, Soybean-derived phospholipids complexed poly (lactic-co-glycolic acid) nanofibrous scaffolds for tissue engineering applications, Mater. Des. 205 (2021), https://doi.org/10.1016/j.matdes.2021.109737 109737.
[13] I.S. Raja, S.H. Lee, M.S. Kang, S.-H. Hyon, A.R. Selvaraj, K. Prabakar, D.-W. Han, The predominant factor influencing cellular behavior on electrospun nanofibrous scaffolds: wettability or surface morphology?, Mater Des. 216 (2022), https://doi.org/10.1016/j.matdes.2022.110580 110580.
[14] S. Anna Paulla, F. Carlise Hannel, R. Andressa, S. Janaina Soares, S. Francisco Trivinho, M. Patrícia Teixeira, J. Henrique Emilio Zorel, S. Mariana de Souza, TiO_2NT as platform for drug release: the effect of film wettability, Orbital: Electron. J. Chem. 11 (6) (2022) 361–366.

[15] E. Terreni, E. Zucchetti, S. Tampucci, S. Burgalassi, D. Monti, P. Chetoni, Combination of nanomicellar technology and in situ gelling polymer as ocular drug delivery system (ODDS) for cyclosporine-A, Pharmaceutics 13 (2) (2021) 192, https://doi.org/10.3390/pharmaceutics13020192.
[16] B. Yang, C. Wei, F. Qian, S. Li, Surface wettability modulated by surfactant and its effects on the drug release and absorption of fenofibrate solid dispersions, AAPS Pharmscitech. 20 (6) (2019) 1–10, https://doi.org/10.1208/s12249-019-1446-4.
[17] S. Ravichandran, J. Radhakrishnan, P. Jayabal, G.D. Venkatasubbu, Antibacterial screening studies of electrospun polycaprolactone nano fibrous mat containing clerodendrum phlomidis leaves extract, Appl. Surf. Sci. 484 (2019) 676–687, https://doi.org/10.1016/j.apsusc.2019.04.150.
[18] S.K. Jaganathan, M.P. Mani, G. Nageswaran, N.P. Krishnasamy, M. Ayyar, The potential of biomimetic nanofibrous electrospun scaffold comprising dual component for bone tissue engineering, Int. J. Polym. Anal. Charact. 24 (3) (2019) 204–218, https://doi.org/10.1080/1023666x.2018.1564127.
[19] N. Akther, S.M. Ali, S. Phuntsho, H. Shon, Surface modification of thin-film composite forward osmosis membranes with polyvinyl alcohol–graphene oxide composite hydrogels for antifouling properties, Desalination 491 (2020), https://doi.org/10.1016/j.desal.2020.114591 114591.
[20] W. Yan, D. Miao, A.A. Babar, J. Zhao, Y. Jia, B. Ding, X. Wang, Multi-scaled interconnected inter- and intra-fiber porous Janus membranes for enhanced directional moisture transport, J. Colloid Interface Sci. 565 (2020) 426–435, https://doi.org/10.1016/j.jcis.2020.01.063.
[21] E. Kosobrodova, A. Kondyurin, V. Solodko, A.S. Weiss, D.R. McKenzie, M.M.M. Bilek, Covalent biofunctionalization of the inner surfaces of a hollow-fiber capillary bundle using packed-bed plasma ion implantation, ACS Appl. Mater. Interfaces 12 (28) (2020) 32163–32174, https://doi.org/10.1021/acsami.0c07070.
[22] L. Gao, T. Kong, Y. Huo, Dual thermoresponsive and pH-responsive poly(vinyl alcohol) derivatives: Synthesis, phase transition study, and functional applications, Macromolecules 49 (19) (2016) 7478–7489, https://doi.org/10.1021/acs.macromol.6b01316.
[23] M.V. Risbud, A.A. Hardikar, S.V. Bhat, R.R. Bhonde, pH-sensitive freeze-dried chitosan–polyvinyl pyrrolidone hydrogels as controlled release system for antibiotic delivery, J. Control. Release 68 (1) (2000) 23–30, https://doi.org/10.1016/S0168-3659(00)00208-X.
[24] S.-Y. Gu, Z.-M. Wang, J.-B. Li, J. Ren, Switchable wettability of thermo-responsive biocompatible nanofibrous films created by electrospinning, Macromol. Mater. Eng. 295 (1) (2010) 32–36, https://doi.org/10.1002/mame.200900215.
[25] Z. Wei, Z. Liu, X. Wang, S. Long, J. Yang, Smart carrier from electrospun core-shell thermo-sensitive ultrafine fibers for controlled drug release, Eur. Polym. J. 114 (2019) 1–10, https://doi.org/10.1016/j.eurpolymj.2019.01.050.
[26] Y. Cheng, G. Cheng, C. Xie, C. Yin, X. Dong, Z. Li, X. Zhou, Q. Wang, H. Deng, Z. Li, Biomimetic silk fibroin hydrogels strengthened by silica nanoparticles distributed nanofibers facilitate bone repair, Adv. Healthcare Mater. 10 (9) (2021) 2001646, https://doi.org/10.1002/adhm.202001646.
[27] D.-G. Yu, Q. Li, W. Song, L. Xu, K. Zhang, T. Zhou, Advanced technique-based combination of innovation education and safety education in higher education, J. Chem. Educ. (2023), https://doi.org/10.1021/acs.jchemed.2c00568.
[28] X. Xu, H. Lv, M. Zhang, M. Wang, Y. Zhou, Y. Liu, D.-G. Yu, Recent progress in electrospun nanofibers and their applications in heavy metal wastewater treatment, Front. Chem. Sci. Eng. (2023) 1–27, https://doi.org/10.1007/s11705-022-2245-0.
[29] Y. Bai, Y. Liu, H. Lv, H. Shi, W. Zhou, Y. Liu, D.-G. Yu, Processes of electrospun polyvinylidene fluoride-based nanofibers, their piezoelectric properties, and several fantastic applications, Polymers 14 (2022) 4311, https://doi.org/10.3390/polym14204311.
[30] Y. Xiao, Y. Fan, W. Tu, Y. Ning, M. Zhu, Y. Liu, X. Shi, Multifunctional PLGA microfibrous rings enable MR imaging-guided tumor chemotherapy and metastasis inhibition through prevention of circulating tumor cell shedding, Nano Today 38 (2021), https://doi.org/10.1016/j.nantod.2021.101123 101123.
[31] D.H. Reneker, I. Chun, Nanometre diameter fibres of polymer, produced by electrospinning, Nanotechnology 7 (3) (1996) 216–223, https://doi.org/10.1088/0957-4484/7/3/009.
[32] P. Zhao, W. Chen, Z. Feng, Y. Liu, P. Liu, Y. Xie, D.-G. Yu, Electrospun nanofibers for periodontal treatment: A recent progress, Int. J. Nanomed. 17 (2022) 4137–4162, https://doi.org/10.2147/IJN.S370340.
[33] Y. Zhou, M. Wang, C. Yan, H. Liu, D.-G. Yu, Advances in the application of electrospun drug-loaded nanofibers in the treatment of oral ulcers, Biomolecules 12 (2022) 1254, https://doi.org/10.3390/biom12091254.
[34] M. Wang, J. Hou, D.-G. Yu, S. Li, J. Zhu, Z. Chen, Electrospun tri-layer nanodepots for sustained release of acyclovir, J. Alloys Compd. 846 (2020). https://doi.org/j.jallcom.2020.156471 156471.
[35] J.F. Cooley, Apparatus for electrically dispersing fluids., U.S. Patents, United States, 1902.
[36] P. Gupta, G.L. Wilkes, Some investigations on the fiber formation by utilizing a side-by-side bicomponent electrospinning approach, Polymer 44 (20) (2003) 6353–6359, https://doi.org/10.1016/S0032-3861(03)00616-5.
[37] D.-G. Yu, J.-J. Li, M. Zhang, G.R. Williams, High-quality Janus nanofibers prepared using three-fluid electrospinning, Chem. Commun. 53 (33) (2017) 4542–4545, https://doi.org/10.1039/C7CC01661A.
[38] M. Cai, H. He, X. Zhang, X. Yan, J. Li, F. Chen, D. Yuan, X. Ning, Efficient synthesis of PVDF/PI side-by-side bicomponent nanofiber membrane with enhanced mechanical strength and good thermal stability, Nanomaterials 9 (1) (2019) 39, https://doi.org/10.3390/nano9010039.
[39] H. Bukhary, G.R. Williams, M. Orlu, Fabrication of electrospun levodopa-carbidopa fixed-dose combinations, Adv. Fiber Mater. 2 (4) (2020) 194–203, https://doi.org/10.1007/s42765-020-00031-1.
[40] R. Ge, Y. Ji, Y. Ding, C. Huang, H. He, D.G. Yu, Electrospun self emulsifying core-shell nanofibers for effective delivery of paclitaxel, Front. Bioeng. Biotechnol. 11 (2023) 1112338, https://doi.org/10.3389/fbioe.2023.1112338.
[41] T. Bujak, T. Wasilewski, Z. Nizioł-Łukaszewska, Role of macromolecules in the safety of use of body wash cosmetics, Colloids and Surfaces B: Biointerfaces 135 (2015) 497–503, https://doi.org/10.1016/j.colsurfb.2015.07.051.
[42] C. Huang, J. Dong, Y. Zhang, S. Chai, X. Wang, S. Kang, D. Yu, P. Wang, Q. Jiang, Gold nanoparticles-loaded polyvinylpyrrolidone/ethylcellulose coaxial electrospun nanofibers with enhanced osteogenic capability for bone tissue regeneration, Mater. Des. 212 (2021), https://doi.org/10.1016/j.matdes.2021.110240 110240.
[43] H. Su, H. Li, H. Lin, X. Shi, Y. Du, Y. Luo, H. Deng, Highly sensitive formaldehyde sensors based on CuO/ZnO composite nanofibrous mats using porous cellulose acetate fibers as templates, Int. J. Biol. Macromol. 206 (2022) 653–660, https://doi.org/10.1016/j.ijbiomac.2022.02.167.
[44] M. KarzarJeddi, O. Laitinen, M. Mahkam, H. Liimatainen, Zwitterionic hybrid aerobeads of binary metal organic frameworks and cellulose nanofibers for removal anionic pollutants, Mater. Des. 196 (2020), https://doi.org/10.1016/j.matdes.2020.109106 109106.
[45] A. Li, Z. Han, Z. Li, J. Li, X. Li, Z. Zhang, A PTHrP-2 loaded adhesive cellulose acetate nanofiber mat as wound dressing accelerates wound healing, Mater. Des. 212 (2021), https://doi.org/10.1016/j.matdes.2021.110241 110241.
[46] D. Edikresnha, T. Suciati, M.M. Munir, K. Khairurrijal, Polyvinylpyrrolidone/cellulose acetate electrospun composite nanofibres loaded by glycerine and garlic extract with in vitro antibacterial activity and release behaviour test, RSC Adv. 9 (45) (2019) 26351–26363, https://doi.org/10.1039/C9RA04072B.
[47] P.B. Tsekova, M.G. Spasova, N.E. Manolova, N.D. Markova, I.B. Rashkov, Electrospun curcumin-loaded cellulose acetate/polyvinylpyrrolidone fibrous materials with complex architecture and antibacterial activity, Mater. Sci. Eng., C 73 (2017) 206–214, https://doi.org/10.1016/j.msec.2016.12.086.
[48] M.M. Castillo-Ortega, A.G. Montaño-Figueroa, D.E. Rodríguez-Félix, G.T. Munive, P.J. Herrera-Franco, Amoxicillin embedded in cellulose acetate-poly (vinyl pyrrolidone) fibers prepared by coaxial electrospinning: Preparation and characterization, Mater. Lett. 76 (2012) 250–254, https://doi.org/10.1016/j.matlet.2012.02.093.
[49] J. Kuczyńska, B. Nieradko-Iwanicka, Future prospects of ketoprofen in improving the safety of the gastric mucosa, Biomed. Pharmacother. 139 (2021), https://doi.org/10.1016/j.biopha.2021.111608 111608.
[50] J. Ju, K. Xiao, X. Yao, H. Bai, L. Jiang, Bioinspired conical copper wire with gradient wettability for continuous and efficient fog collection, Adv. Mater. 25 (41) (2013) 5937–5942, https://doi.org/10.1002/adma.201301876.
[51] H. He, M. Wu, J. Zhu, Y. Yang, R. Ge, D.-G. Yu, Engineered spindles of little molecules around electrospun nanofibers for biphasic drug release, Adv. Fiber Mater. 4 (2) (2022) 305–317, https://doi.org/10.1007/s42765-021-00112-9.
[52] W. Jiang, X. Zhang, P. Liu, Y. Zhang, W. Song, D.-G. Yu, X. Lu, Electrospun healthcare nanofibers from medicinal liquor of Phellinus igniarius, Adv. Compos. Hybrid Mater. 5 (2022) 3045–3056, https://doi.org/10.1007/s42114-022-00551-x.
[53] H. Lv, S. Guo, G. Zhang, W. He, Y. Wu, D.-G. Yu, Electrospun structural hybrids of acyclovir-polyacrylonitrile at acyclovir for modifying drug release, Polymers 13 (2021) 4286, https://doi.org/10.3390/polym13244286.
[54] Y. Wang, D.G. Yu, Y. Liu, Y.N. Liu, Progress of electrospun nanofibrous carriers for modifications to drug release profiles, J. Funct. Biomater. 13 (2022) 289, https://doi.org/10.3390/jfb13040289.
[55] A.M. Abdelghany, M.S. Mekhail, E.M. Abdelrazek, M.M. Aboud, Combined DFT/FTIR structural studies of monodispersed PVP/Gold and silver nano particles, J. Alloys Compd. 646 (2015) 326–332, https://doi.org/10.1016/j.jallcom.2015.05.262.
[56] A.W. Jatoi, I.S. Kim, Q.-Q. Ni, Cellulose acetate nanofibers embedded with AgNPs anchored TiO_2 nanoparticles for long term excellent antibacterial applications, Carbohydr. Polym. 207 (2019) 640–649, https://doi.org/10.1016/j.carbpol.2018.12.029.
[57] L. Wei, J. Song, B. Cheng, Z. Yang, Synthesis, characterization and antibacterial properties of novel cellulose acetate sorbate, Carbohydr. Polym. 243 (2020), https://doi.org/10.1016/j.carbpol.2020.116416 116416.
[58] S. Kang, S. Hou, X. Chen, D.-G. Yu, L. Wang, X. Li, G.R. Williams, Energy-saving electrospinning with a concentric Teflon-core rod spinneret to create medicated nanofibers, Polymers 12 (2020) 2421, https://doi.org/10.3390/polym12102421.
[59] R. Soto, M. Svärd, V. Verma, L. Padrela, K. Ryan, Å.C. Rasmuson, Solubility and thermodynamic analysis of ketoprofen in organic solvents, Int. J. Pharm. 588 (2020), https://doi.org/10.1016/j.ijpharm.2020.119686 119686.
[60] J. Hou, Y. Wang, H. Xue, Y. Dou, Biomimetic growth of hydroxyapatite on electrospun CA/PVP core–shell nanofiber membranes, Polymers 10 (9) (2018) 1032, https://doi.org/10.3390/polym10091032.
[61] N.T. Chamakos, D.G. Sema, A.G. Papathanasiou, Progress in modeling wetting phenomena on structured substrates, Arch. Comput. Method Eng. 28 (3) (2021) 1647–1666, https://doi.org/10.1007/s11831-020-09431-3.
[62] H. Gao, J. Feng, Y. Pi, Z. Zhou, B. Zhang, Y. Wu, X. Wang, X. Jiang, L. Jiang, Bandgap engineering of single-crystalline perovskite arrays for high-

performance photodetectors, Adv. Funct. Mater. 28 (46) (2018) 1804349, https://doi.org/10.1002/adfm.201804349.
[63] Y. Li, J. Huang, J. Cheng, S. Xu, P. Pi, X. Wen, Enhanced movement of two-component droplets on a wedge-shaped Ag/Cu surface by a wettability gradient, ACS Appl. Mater. Interfaces 13 (13) (2021) 15857–15865, https://doi.org/10.1021/acsami.1c00517.